PRAMANA — journal of physics

Vol. 83, No. 5
November 2014
pp. 651–659

The Hoyle state in nuclear lattice effective field theory

TIMO A LÄHDE[1,*], EVGENY EPELBAUM[2], HERMANN KREBS[2], DEAN LEE[3], ULF-G MEIßNER[1,4,5] and GAUTAM RUPAK[6]

[1]Institute for Advanced Simulation, Institut für Kernphysik, and Jülich Center for Hadron Physics, Forschungszentrum Jülich, D-52425 Jülich, Germany
[2]Institut für Theoretische Physik II, Ruhr-Universität Bochum, D-44870 Bochum, Germany
[3]Department of Physics, North Carolina State University, Raleigh, NC 27695, USA
[4]Helmholtz-Institut für Strahlen-und Kernphysik and Bethe Center for Theoretical Physics, Universität Bonn, D-53115 Bonn, Germany
[5]JARA–High Performance Computing, Forschungszentrum Jülich, D-52425 Jülich, Germany
[6]Department of Physics and Astronomy, Mississippi State University, Mississippi State, MS 39762, USA
*Corresponding author. E-mail: t.laehde@fz-juelich.de

DOI: 10.1007/s12043-014-0861-z; ***e*Publication:** 8 October 2014

Abstract. We review the calculation of the Hoyle state of ^{12}C in nuclear lattice effective field theory (NLEFT) and its anthropic implications in the nucleosynthesis of ^{12}C and ^{16}O in red giant stars. We also analyse the extension of NLEFT to the regime of medium-mass nuclei, with emphasis on the determination of the ground-state energies of the α nuclei ^{16}O, ^{20}Ne, ^{24}Mg, and ^{28}Si by Euclidean time projection. Finally, we discuss recent NLEFT results for the spectrum, electromagnetic properties, and α-cluster structure of ^{16}O.

Keywords. Nuclear structure; chiral effective field theory; lattice Monte Carlo.

PACS Nos 21.10.Dr; 21.30.−x; 21.60.De

1. Introduction

Nuclear lattice effective field theory (NLEFT) is a first-principles approach, in which chiral EFT for nucleons is combined with numerical auxiliary-field quantum Monte Carlo (AFQMC) lattice calculations. NLEFT differs from other *ab-initio* methods [1–6] in that it is an unconstrained Monte Carlo calculation, which does not rely on truncated basis expansions, many-body perturbation theory, or on prior information about the structure of the nuclear wave function.

As in chiral EFT, our calculations are organized in powers of a generic soft scale Q associated with factors of momenta and the pion mass [7]. We denote $\mathcal{O}(Q^0)$ as leading order (LO), $\mathcal{O}(Q^2)$ as next-to-leading order (NLO), and $\mathcal{O}(Q^3)$ as next-to-next-to-leading

order (NNLO) contributions. The present calculations are performed upto NNLO. We define $H_{\rm LO}$ as the LO lattice Hamiltonian and $H_{SU(4)}$ as the equivalent Hamiltonian with the pion–nucleon coupling $g_A = 0$ and contact interactions that respect Wigner's $SU(4)$ symmetry.

In our NLEFT calculations, $H_{\rm LO}$ is treated non-perturbatively (see [8] for a review). The NLO contribution to the two-nucleon force (2NF), the electromagnetic and strong isospin-breaking contributions (EMIB), and the three-nucleon force (3NF) which first enters at NNLO, are all treated as perturbations. It should be noted that our 'LO' calculations use smeared short-range interactions that capture much of the corrections usually treated at NLO and higher orders [9]. At NNLO, the 3NF overbinds nuclei with $A \geq 4$ due to a clustering instability which involves four nucleons on the same lattice site. A long-term objective of NLEFT is to remedy this problem by decreasing the lattice spacing and including the next-to-next-to-next-to-leading order (N3LO) corrections in chiral EFT. Simultaneously, the overbinding problem has been rectified by means of a 4N contact interaction, tuned to the empirical binding energy of either ^{4}He or ^{8}Be [10]. While this provides a good description of the α nuclei upto $A = 12$ including the Hoyle state [10–12], the overbinding is found to increase more rapidly for $A \geq 16$. In [13], a non-local $4N$ interaction which accounts for all possible configurations of four nucleons on adjacent lattice sites was introduced, and adjusted to the empirical binding energy of ^{24}Mg. A detailed study of the spectrum and electromagnetic properties of ^{16}O (with the inclusion of the effective $4N$ interaction) is reported in [14].

2. The Hoyle state

The Hoyle state is a resonance with spin-parity quantum numbers $J^p = 0^+$ in the spectrum of ^{12}C, which plays an important role in resonantly enhancing the reaction rate for the so-called triple-α process, which is responsible for the production of carbon in massive stars that have reached the red giant stage in their evolution. This reaction represents a significant bottleneck in the stellar nucleosynthesis, as ^{8}Be is an unstable (though relatively long-lived) resonance. For ^{12}C to form, a third α-particle must combine with the ^{8}Be resonance to create the Hoyle state, which subsequently decays electromagnetically to the ground state of ^{12}C. This reaction may then proceed further (non-resonantly) to form ^{16}O by the addition of a fourth α-particle. However, the temperature of the stellar plasma at which the triple-α process takes place depends exponentially on the energy Δ_h of the Hoyle state above the triple-α threshold, which is experimentally known as $\Delta_h \simeq 379.5$ keV. Stellar model calculations [15] have shown that only a narrow window of ± 100 keV exists in Δ_h, where significant amounts of carbon and oxygen can be produced simultaneously.

Our NLEFT calculations [12] have recently shed light on the structure, electromagnetic properties, and transitions of the Hoyle state from first principles, and have furthermore enabled an initial investigation of the sensitivity of the triple-α process to changes in the fundamental parameters, such as the light quark mass $m_{\rm q}$ and the electromagnetic fine-structure constant $\alpha_{\rm em}$. In particular, carbon–oxygen-based life as we know appears unlikely to become strongly disfavoured for relative changes smaller than $\simeq 3\%$ in $m_{\rm q}$ or $\alpha_{\rm em}$. This situation, where the production rates of ^{12}C and ^{16}O are not excessively fine-tuned, arises due to strong correlations between the binding energy of ^{4}He and the energies of the ^{8}Be and Hoyle state resonances. In turn, this is a reflection of the

Table 1. Lattice results at leading order (LO) and available experimental values for the root-mean-square charge radii and quadrupole moments of the ^{12}C states.

	LO	Exp.
$r(0_1^+)$ (fm)	2.2(2)	2.47(2) [17]
$r(2_1^+)$ (fm)	2.2(2)	–
$Q(2_1^+)$ (e fm^2)	6(2)	6(3) [18]
$r(0_2^+)$ (fm)	2.4(2)	–
$r(2_2^+)$ (fm)	2.4(2)	–
$Q(2_2^+)$ (e fm^2)	−7(2)	–

Table 2. Lattice results at leading order (LO) and available experimental values for electromagnetic transitions involving the even-parity states of ^{12}C.

	LO	Exp.
$B(E2, 2_1^+ \to 0_1^+)$ (e^2 fm^4)	5(2)	7.6(4) [19]
$B(E2, 2_1^+ \to 0_2^+)$ (e^2 fm^4)	1.5(7)	2.6(4) [19]
$B(E2, 2_2^+ \to 0_1^+)$ (e^2 fm^4)	2(1)	–
$B(E2, 2_2^+ \to 0_2^+)$ (e^2 fm^4)	6(2)	–
$M(E0, 0_2^+ \to 0_1^+)$ (e^2 fm^4)	3(1)	5.5(1) [20]

underlying α-cluster structure of the Hoyle state, which is found to resemble a 'bent-arm' or obtuse triangular configuration. However, such calculations also require some knowledge on how the LO contact terms in the chiral EFT interaction depend on m_q or, equivalently, on the pion mass m_π. At present, this information enters through the derivatives of the two-nucleon S-wave scattering lengths in the singlet and triplet channels, $\partial a_s^{-1}/\partial m_\pi$ and $\partial a_t^{-1}/\partial m_\pi$, respectively. So far, these have been difficult to determine accurately from lattice QCD calculations. In this situation, the derivatives of the binding energies $\partial B_3/\partial m_\pi$ and $\partial B_4/\partial m_\pi$ of ^{3}He and ^{4}He may prove more constraining in the near term, as these are easier to extrapolate to the physical point from lattice QCD data [16]. NLEFT work in this direction is in progress.

Finally, we briefly review our results for the electromagnetic properties of the low-lying even-parity states of ^{12}C in table 1 and our results for the electromagnetic transitions between these states in table 2. These are currently available to LO (the extension to NNLO will appear in a future publication). We note that the good agreement with experimental results (where available) inspires confidence in our conclusions concerning the α-cluster structure and possible anthropic role of the Hoyle state.

3. Medium-mass nuclei in NLEFT

Recently, much effort has been directed towards the extension of NLEFT beyond ^{12}C into the regime of medium-mass nuclei (see in particular [13]). In this section, we shall

review the developments in computational methods which have made this extension possible. At present, our calculations have been performed with a (spatial) lattice spacing of $a = 1.97$ fm in a periodic cube of length $L = 11.8$ fm. In [13], our trial wave function $|\Psi_A^{\text{init}}\rangle$ is a Slater-determinant state composed of delocalized standing waves, with A nucleons and the desired spin and isospin. First, we project $|\Psi_A^{\text{init}}\rangle$ for a time t' using the Euclidean-time evolution operator of the $SU(4)$ Hamiltonian, giving the 'trial state' $|\Psi_A(t')\rangle \equiv \exp(-H_{SU(4)}t')|\Psi_A^{\text{init}}\rangle$. Second, we use the full Hamiltonian H_{LO} to construct the Euclidean-time projection amplitude

$$Z_A(t) \equiv \langle\Psi_A(t')|\exp(-H_{\text{LO}}t)|\Psi_A(t')\rangle, \tag{1}$$

and the 'transient energy'

$$E_A(t) = -\partial[\ln Z_A(t)]/\partial t. \tag{2}$$

If we denote the lowest (normalizable) eigenstate of H_{LO} by $|\Psi_{A,0}\rangle$ which has a non-vanishing overlap with the trial state $|\Psi_A(t')\rangle$, we obtain the corresponding energy $E_{A,0}$ as the $t \to \infty$ limit of $E_A(t)$. The NLO and NNLO contributions are evaluated in perturbation theory. We compute operator expectation values using

$$Z_A^{\mathcal{O}}(t) \equiv \langle\Psi_A(t')|\exp(-H_{\text{LO}}t/2)\mathcal{O}\exp(-H_{\text{LO}}t/2)|\Psi_A(t')\rangle \tag{3}$$

for any operator $\mathcal{O}$. Given the ratio $X_A^{\mathcal{O}}(t) = Z_A^{\mathcal{O}}(t)/Z_A(t)$, the expectation value of $\mathcal{O}$ for the desired state $|\Psi_{A,0}\rangle$ is obtained as $X_{A,0}^{\mathcal{O}} \equiv \langle\Psi_{A,0}|\mathcal{O}|\Psi_{A,0}\rangle = \lim_{t\to\infty} X_A^{\mathcal{O}}(t)$.

Sign oscillations make it difficult to reach sufficiently large values of the projection time t. It is helpful to note that the closer the trial state $|\Psi_A(t')\rangle$ is to $|\Psi_{A,0}\rangle$, the less is the necessary projection time t. $|\Psi_A(t')\rangle$ can be optimized by adjusting both the $SU(4)$ projection time t' and the strength of the coupling $C_{SU(4)}$ of $H_{SU(4)}$. The accuracy of the extrapolation $t \to \infty$ can be further improved by simultaneously incorporating data from trial states that differ in $C_{SU(4)}$. The large-time behaviour of $Z_A(t)$ and $Z_A^{\mathcal{O}}(t)$ is controlled by the low-energy spectrum of H_{LO}. Let $|E\rangle$ denote the eigenstates of H_{LO} with energy E and let $\rho_A(E)$ denote the density of states for a system of A nucleons. We then express $Z_A(t)$ and $Z_A^{\mathcal{O}}(t)$ in terms of their spectral representations

$$Z_A(t) = \int \mathrm{d}E\ \rho_A(E)\left|\langle E|\Psi_A(t')\rangle\right|^2 \exp(-Et), \tag{4}$$

$$Z_A^{\mathcal{O}}(t) = \int \mathrm{d}E\,\mathrm{d}E'\,\rho_A(E)\,\rho_A(E')\langle\Psi_A(t')|E\rangle\,\langle E|\mathcal{O}|E'\rangle \times\langle E'|\Psi_A(t')\rangle\ \exp(-(E+E')t/2) \tag{5}$$

from which we construct the spectral representations of $E_A(t)$ and $X_A^{\mathcal{O}}(t)$. We can approximate these to arbitrary accuracy over any finite range of t by taking $\rho_A(E)$ to be a sum of energy delta functions $\rho_A(E) \approx \sum_{i=0}^{i_{\max}} \delta(E - E_{A,i})$, where we take $i_{\max} = 4$ for the ^{4}He ground state and $i_{\max} = 3$ for $A \geq 8$. Using the data obtained for different values of $C_{SU(4)}$, we perform a correlated fit of $E_A(t)$ and $X_A^{\mathcal{O}}(t)$ for all operators $\mathcal{O}$ that contribute to the NLO and NNLO energy corrections. We find that the use of 2–6 trial states allows for a much more precise determination of $E_{A,0}$ and $X_{A,0}^{\mathcal{O}}$ than hitherto possible. In particular, we may 'triangulate' $X_{A,0}^{\mathcal{O}}$ using trial states that correspond to functions $X_A^{\mathcal{O}}(t)$ which converge both from above and below.

4. Lattice Monte Carlo results for NLEFT with $A \geq 16$

In this section, we discuss the NLEFT results for nuclei in the medium-mass range (see also [13,14]). A detailed description of the NLEFT calculation for ^{16}O is given in figure 1, while the results for the α nuclei from ^{4}He to ^{28}Si are shown in table 3. The curves in figure 1 show a correlated fit for all trial states, using the same spectral density $\rho_A(E)$. The upper row shows (from left to right) the LO energy, the total isospin-symmetric 2NF correction (NLO), the electromagnetic and isospin-breaking corrections (EMIB), and the total 3NF correction. The remaining panels show the matrix elements $X_A^{\mathcal{O}}(t)$ that form part of

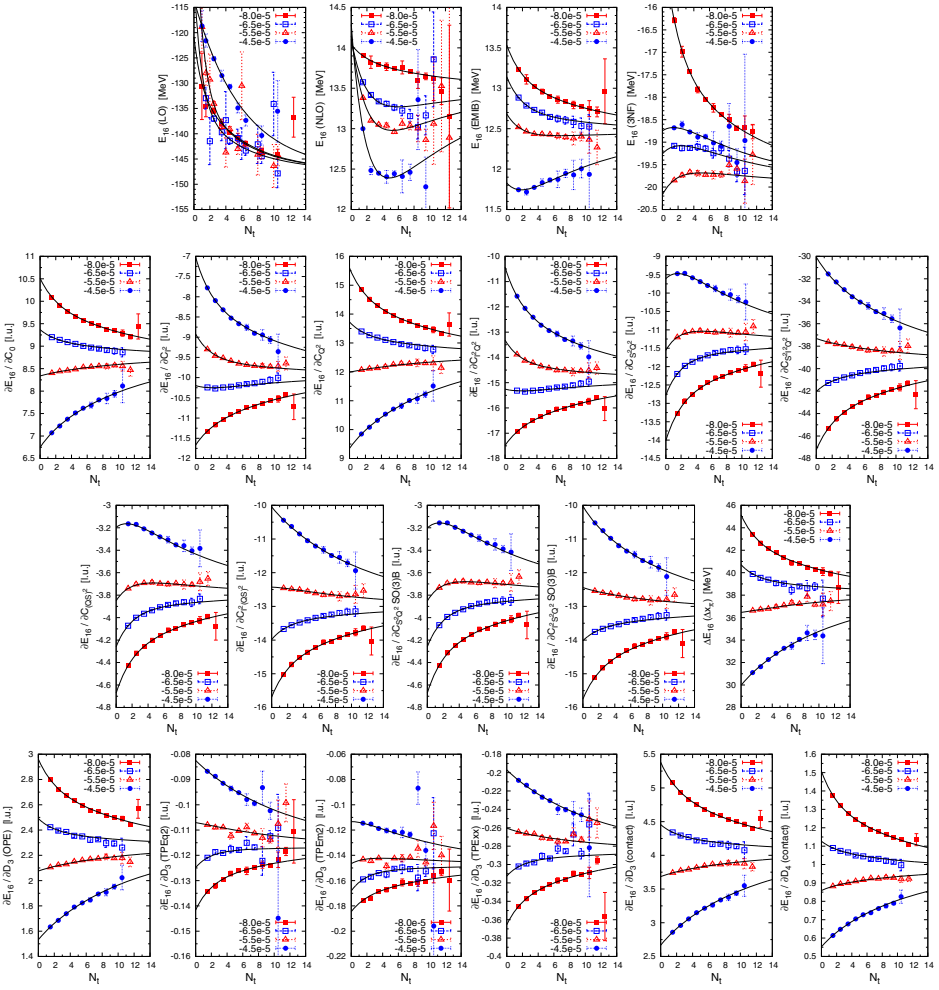

Figure 1. NLEFT results for ^{16}O. The LO energy $E_{\rm LO} = -147.3(5)$ MeV and the result at NNLO including $4N$ interactions is $E_{\rm NNLO+4N} = -131.3(5)$ MeV. The empirical binding energy is -127.62 MeV (for definitions, see text).

Table 3. NLEFT results for the ground-state energies (in MeV). The combined statistical and extrapolation errors are given in parentheses. The columns labelled 'LO($2N$)' and 'NNLO($2N$)' show the energies at each order using the two-nucleon force only. The column labelled '$+3N$' also includes the 3NF, which first appears at NNLO. Finally, the column '$+4N_{\text{eff}}$' includes the 'effective' $4N$ force. The column 'Exp.' gives the empirical energies.

A	LO($2N$)	NNLO($2N$)	$+3N$	$+4N_{\text{eff}}$	Exp.
4	−28.87(6)	−25.60(6)	−28.93(7)	−28.93(7)	−28.30
8	−57.9(1)	−48.6(1)	−56.4(2)	−56.3(2)	−56.35
12	−96.9(2)	−78.7(2)	−91.7(2)	−90.3(2)	−92.16
16	−147.3(5)	−121.4(5)	−138.8(5)	−131.3(5)	−127.62
20	−199.7(9)	−163.6(9)	−184.3(9)	−165.9(9)	−160.64
24	−253(2)	−208(2)	−232(2)	−198(2)	−198.26
28	−330(3)	−275(3)	−308(3)	−233(3)	−236.54

the NLO and 3NF terms. The operators $\partial E_A/\partial C_i$ give the contributions of the NLO contact interactions and $\Delta E_A(\Delta x_\pi)$ denotes the energy shift due the $\mathcal{O}(a^2)$-improved pion–nucleon coupling. The operators $\partial E_A/\partial D_i$ give individual contributions to the total 3NF correction.

From the results in table 3, we note that the NNLO results are good upto $A = 12$, at which point an increasing overbinding manifests itself for $A \geq 16$. As we ascend the α ladder from ^{4}He to ^{28}Si, the lighter nuclei can be described as collections of α-clusters [11,12]. As the number of clusters increases, they become increasingly densely packed, such that a more uniform liquid of nucleons is approached. This increase in the density of α-clusters appears correlated with the gradual overbinding we observe at NNLO for $A \geq 16$. As this effect becomes noticeable for ^{16}O, we can view it as a problem which first arises in a system of four α-clusters.

Following [10], which removed discretization errors associated with four nucleons occupying the same lattice site, we can attempt to remove similar errors associated with four α-clusters in close proximity with neighbouring lattice sites. In table 3, the column labelled '$+4N_{\text{eff}}$' shows the results at NNLO while including both the 3NF and the 'effective' nearest-neighbour $4N$ interaction $V^{(4N_{\text{eff}})}$. Due to the low momentum cutoff (corresponding to a lattice spacing of $a = 1.97$ fm), the two-pion exchange contributions have been absorbed into the contact interactions at NLO. We have tuned the coupling $D^{(4N_{\text{eff}})}$ of $V^{(4N_{\text{eff}})}$ to give approximately the correct energy for the ground state of ^{24}Mg. With $V^{(4N_{\text{eff}})}$ included, a good description of the ground-state energies is obtained over the full range from light to medium-mass nuclei, with a maximum error no larger than $\sim$3%. This lends support to the qualitative picture that the overbinding at NNLO in table 3 is associated with the increased packing of α-clusters and the eventual crossover to a uniform nucleon liquid. The missing physics would then be comprised of short-range repulsive forces that counteract the dense packing of α-clusters.

In spite of the good agreement (upon introduction of $V^{(4N_{\text{eff}})}$) with experiment in table 3, we also need to verify that the good description of the binding energies is not accidental. It is then helpful to check whether a consistent picture is obtained with respect to excited

states, transitions, and electromagnetic properties of nuclei in the medium-mass range where $V^{(4N_{\rm eff})}$ gives a sizable contribution.

5. Alpha-cluster structure of ^{16}O

Since the early work of Wheeler [21], theoretical studies of ^{16}O have been based on α-cluster models [22–28] and some experimental evidence for α-particle substructure in ^{16}O has been found from the analysis of decay products [29]. While some of the puzzles in the structure of ^{16}O have been explained on a phenomenological (or geometrical) level, so far no support has been available for the α-cluster structure of ^{16}O from *ab-initio* calculations. The NLEFT results for ^{16}O have been reported in [14], which is also the first time that evidence for the tetrahedral α-cluster structure of the ground state of ^{16}O has been found from an *ab-initio* calculation. We have also found the first excited 0^+ state of ^{16}O to predominantly consist of a square arrangement of α-clusters. We summarize the results for the electromagnetic properties and transition rates in ^{16}O in tables 4 and 5.

The computed charge radii, quadrupole moments, and transition rates of ^{16}O provide very convincing evidence supporting the realism of our extension of NLEFT to medium-mass nuclei. In particular, the excitation energies and level ordering in ^{16}O (see table 4) are found to be very sensitive to the strength and form of $V^{(4N_{\rm eff})}$. This sensitivity arises due to the differences in the α-cluster structure of the states in question. We also note that NLEFT is able to explain the empirical value of $B(E2, 2_1^+ \to 0_2^+)$, which is $\simeq$30 times larger than the Weisskopf single-particle shell model estimate (see table 5). This provides confirmation of the interpretation of the 2_1^+ state as a rotational excitation of the 0_2^+ state. Finally, we provide a prediction for the quadrupole moment of the 2_1^+ state. We note that the NLEFT calculation of the electromagnetic transitions requires a full coupled-channel analysis. For such calculations, we use initial states that consist of a compact triangle of α-clusters and a fourth α-cluster, located either in the plane of the triangle (square-like) or out of the plane of the triangle (tetrahedral).

In table 5, we note that the LO charge radius $r_{\rm LO}$ of the ground state of ^{16}O is smaller than the empirical value $r_{\rm exp}$. This leads to a systematic deviation, which arises from the overall size of the second moment of the charge distribution. To compensate for this overall scaling mismatch, we have also calculated 'rescaled' quantities multiplied by powers of the ratio $r_{\rm exp}/r_{\rm LO}$, according to the length dimension of each observable. With such a scaling factor included, we find that the NLEFT predictions for the $E2$ and $E0$ transitions are in good agreement with the available experimental values.

Table 4. NLEFT results and experimental (Exp.) energies for the lowest even-parity states of ^{16}O (in MeV). The errors are one-standard-deviation estimates which include statistical Monte Carlo errors and uncertainties due to the extrapolation $N_t \to \infty$.

J_n^p	LO(2N)	NNLO(2N)	+3N	+4$N_{\rm eff}$	Exp.
0_1^+	−147.3(5)	−121.4(5)	−138.8(5)	−131.3(5)	−127.62
0_2^+	−145(2)	−116(2)	−136(2)	−123(2)	−121.57
2_1^+	−145(2)	−116(2)	−136(2)	−123(2)	−120.70

Table 5. NLEFT results for the charge radius r, the quadrupole moment Q, and the electromagnetic transition amplitudes for $E2$ and $E0$ transitions, as defined in [30]. We compare with empirical (Exp.) values where these are known. For the quadrupole moment and the transition amplitudes, we also show 'rescaled' LO results, which correct for the deviation from the empirical value of the charge radius at LO (see text). The errors are one-standard-deviation estimates which include statistical Monte Carlo errors and uncertainties due to the extrapolation $N_t \to \infty$.

	LO	Rescaled	Exp.
$r(0_1^+)$ (fm)	2.3(1)	–	2.710(15) [31]
$r(0_2^+)$ (fm)	2.3(1)	–	–
$r(2_1^+)$ (fm)	2.3(1)	–	–
$Q(2_1^+)$ (e fm^2)	10(2)	15(3)	–
$B(E2, 2_1^+ \to 0_2^+)$ (e^2 fm^4)	22(4)	46(8)	65(7) [19]
$B(E2, 2_1^+ \to 0_1^+)$ (e^2 fm^4)	3.0(7)	6.2(1.6)	7.4(2) [32]
$M(E0, 0_2^+ \to 0_1^+)$ (e fm^4)	2.1(7)	3.0(1.4)	3.6(2) [33]

6. Conclusions and outlook

We have presented an overview of the central NLEFT results for the low-lying even-parity spectra of ^{12}C and ^{16}O. This includes the Hoyle state of ^{12}C which plays a central role in the stellar nucleosynthesis of life-essential elements. We have also shown that the electromagnetic properties and transition rates of ^{12}C and ^{16}O are in agreement with the available experimental data. While the long-term objectives of NLEFT are to decrease the lattice spacing and include higher orders in the EFT expansion, we also find that the missing physics upto ^{28}Si can be approximated by an 'effective' 4N interaction. These results represent an important step towards more comprehensive NLEFT calculations of medium-mass nuclei in the near future.

Acknowledgements

The authors are grateful for the help in automated data collection by Thomas Luu. Partial financial support from the Deutsche Forschungsgemeinschaft (Sino-German CRC 110), the Helmholtz Association (Contract No. VH-VI-417), BMBF (Grant No. 05P12PDFTE), and the US Department of Energy (DE-FG02-03ER41260) is acknowledged. This work was further supported by the EU HadronPhysics3 project and funds provided by the ERC Project No. 259218 NUCLEAREFT. The computational resources were provided by the Jülich Supercomputing Centre at the Forschungszentrum Jülich and by RWTH Aachen.

References

[1] G Hagen, M Hjorth-Jensen, G R Jansen, R Machleidt and T Papenbrock, *Phys. Rev. Lett.* **109**, 032502 (2012)

[2] E D Jurgenson, P Maris, R J Furnstahl, P Navratil, W E Ormand and J P Vary, *Phys. Rev. C* **87**, 054312 (2013)
[3] R Roth, J Langhammer, A Calci, S Binder and P Navratil, *Phys. Rev. Lett.* **107**, 072501 (2011)
[4] H Hergert, S K Bogner, S Binder, A Calci, J Langhammer, R Roth and A Schwenk, *Phys. Rev. C* **87**, 034307 (2013)
[5] A Lovato, S Gandolfi, R Butler, J Carlson, E Lusk, S C Pieper and R Schiavilla, *Phys. Rev. Lett.* **111**, 092501 (2013)
[6] V Somà, C Barbieri and T Duguet, *Phys. Rev. C* **87**, 011303(R) (2013)
[7] E Epelbaum, H-W Hammer and Ulf-G Meißner, *Rev. Mod. Phys.* **81**, 1773 (2009)
[8] D Lee, *Prog. Part. Nucl. Phys.* **63**, 117 (2009)
[9] B Borasoy, E Epelbaum, H Krebs, D Lee and Ulf-G Meißner, *Eur. Phys. J. A* **31**, 105 (2007)
[10] E Epelbaum, H Krebs, D Lee and Ulf-G Meißner, *Phys. Rev. Lett.* **104**, 142501 (2010); *ibid.*, *Eur. Phys. J. A* **45**, 335 (2010)
[11] E Epelbaum, H Krebs, D Lee and Ulf-G Meißner, *Phys. Rev. Lett.* **106**, 192501 (2011)
[12] E Epelbaum, H Krebs, T A Lähde, D Lee and Ulf-G Meißner, *Phys. Rev. Lett.* **109**, 252501 (2012); *ibid.*, *Phys. Rev. Lett.* **110**, 112502 (2013); *ibid.*, *Eur. Phys. J. A* **49**, 82 (2013)
[13] T A Lähde, E Epelbaum, H Krebs, D Lee, Ulf-G Meißner and G Rupak, *Phys. Lett. B* **732**, 110 (2014)
[14] E Epelbaum, H Krebs, T A Lähde, D Lee, Ulf-G Meißner and G Rupak, *Phys. Rev. Lett.* **112**, 102501 (2014)
[15] H Schlattl, A Heger, H Oberhummer, T Rauscher and A Csótó, *Astrophys. Space Sci.* **291**, 27 (2004)
[16] S R Beane, S D Cohen, W Detmold, H-W Lin and M J Savage, *Phys. Rev. D* **89**, 074505 (2014)
[17] L A Schaller *et al*, *Nucl. Phys. A* **379**, 523 (1982)
[18] W J Vermeer *et al*, *Phys. Lett. B* **122**, 23 (1983)
[19] F Ajzenberg-Selove, *Nucl. Phys. B* **506**, 1 (1990)
[20] M Chernykh *et al*, *Phys. Rev. Lett.* **105**, 022501 (2010)
[21] J A Wheeler, *Phys. Rev.* **52**, 1083 (1937)
[22] D M Dennison, *Phys. Rev.* **96**, 378 (1954)
[23] H Feshbach and F Iachello, *Phys. Lett. B* **45**, 7 (1973)
[24] D Robson, *Phys. Rev. Lett.* **42**, 876 (1979)
[25] W Bauhoff, H Schultheis and R Schultheis, *Phys. Rev. C* **29**, 1046 (1984)
[26] I N Filikhin and S L Yakovlev, *Phys. Atom. Nucl.* **64**, 409 (2000)
[27] A Tohsaki, H Horiuchi, P Schuck and G Röpke, *Phys. Rev. Lett.* **87**, 192501 (2001)
[28] R Bijker, *AIP Conf. Proc.* **1323**, 28 (2010); *ibid.*, *J. Phys.: Conf. Ser.* **380**, 012003 (2012)
[29] CHARISSA Collaboration: M Freer, *J. Phys. G* **31**, S1795 (2005)
[30] A Bohr and B R Mottelson, *Nuclear structure. Single-particle motion* (W A Benjamin, New York, 1969) Vol. I
[31] J C Kim *et al*, *Nucl. Phys. A* **297**, 301 (1978)
[32] R Moreh, W C Sellyey, D Sutton and R Vodhanel, *Phys. Rev. C* **31**, 2314 (1985)
[33] H Miska *et al*, *Phys. Lett. B* **58**, 155 (1975)